Geomorphology 367 (2020) 107296

Contents lists available at ScienceDirect

Geomorphology

journal homepage: www.elsevier.com/locate/geomorph

Which geomorphic processes can be informed by luminescence measurements?

N.D. Brown *

Department of Earth and Planetary Science, University of California, Berkeley, CA, USA
Berkeley Geochronology Center, 2455 Ridge Road, Berkeley, CA, USA

ARTICLE INFO

Article history:
Received 1 April 2020
Received in revised form 3 June 2020
Accepted 10 June 2020
Available online xxxx

Keywords:
Luminescence
OSL
Geochronology

ABSTRACT

Luminescence signals from quartz and feldspar contain a wealth of information about exposure to heat and sunlight. While many studies have focused on quantifying individual processes such as grain transport and burial, cooling during exhumation, or bleaching of freshly exposed rock surfaces, not much work has yet been done to illustrate how these effects might interact. For example, how might a geomorphologist interpret the luminescence signals within a riverine cobble or within a recent rockfall from an uplifting terrain? This study attempts to address this issue by first presenting a simple kinetic expression for OSL signal accumulation in response to background radiation, and OSL loss by exposure to heat or to direct or attenuated sunlight. This model is then used to simulate three example sample histories. Simulation results demonstrate how much information can be embedded within one sample's luminescence signal and how disparate geomorphic histories can produce strikingly similar signals. The temperatures and timescales which can be examined with luminescence signals are presented in comparison to those of various geomorphic processes. Finally, simulation results illustrate the benefit of using signals of different stability to better understand a sample's recent geologic history.

1. Introduction

Geomorphologists have become increasingly aware that optically stimulated luminescence (OSL) signals from silt, sand, cobbles, and rock outcrops contain detailed information about a sample's exposure to sunlight, heat, or both. Luminescence signals grow on timescales of hundreds to several hundred thousand years and deplete at a range of rates, depending on the signal resetting mechanism. For example, exposure to direct sunlight or mid-crustal temperatures will eliminate built-up signals in a matter of seconds or minutes, but exposure to attenuated sunlight or upper-crustal temperatures may reduce the signal over many millennia. From the perspective of an individual grain, many geomorphic processes produce changes in sunlight or heat exposure (Fig. 1). Three examples illustrate this point. Floods remobilize packages of old, buried grains. These grains may travel downstream, occasionally rising in the water column to see filtered sunlight for the first time since they were originally buried. Later, these grains may wash up onto dry ground, into full daylight, finally losing all remnant signal. On slower timescales, grains in a soil profile may incrementally work their way up to the sunlit surface with the help of root growth or burrowing animals before eventually sinking back into the dark soil. Tectonic uplift can also drive grains closer to the surface as overburden rock is eroded away. The cooling experienced by these rising grains slows their loss of signal and they begin to retain an OSL signal.

There has been much work recently using luminescence signals to measure a variety of tectonic and geomorphic signals, including hard rock erosion rates (Sohbati et al., 2018; Brown and Moon, 2019), surface exposure ages (Sohbati et al., 2012, 2015; Freiesleben et al., 2015; Lehmann et al., 2018; Gliganic et al., 2019), soil mixing rates (Heimsath et al., 2002; Johnson et al., 2014; Reimann et al., 2017; Furbish et al., 2018b; Román-Sánchez et al., 2019a, 2019b; Gray et al., 2020), bedrock temperatures and cooling rates (Herman et al., 2010; Guralnik et al., 2015b; Schmidt et al., 2015; King et al., 2016b, 2016c; Brown et al., 2017; Brown and Rhodes, 2017; Biswas et al., 2018), stream transport rates (McGuire and Rhodes, 2015a, 2015b; Gray and Mahan, 2015; Gray et al., 2017, 2018), delta evolution (Shen et al., 2015; Chamberlain et al., 2017, 2018, 2020), sand dune dynamics (Fujioka et al., 2009; Bristow et al., 2010; Hesse, 2016; Zular et al., 2020), landslide chronologies (Lang et al., 1999; Balescu et al., 2007; Del Vecchio et al., 2018), wildfire timing and intensity (Rhodes et al., 2004; Rengers et al., 2017), terrace aggradation and abandonment (Fuller et al., 2009; Brown et al., 2015; Malatesta et al., 2017), earthquake recurrence intervals (Salisbury et al., 2018; Zinke et al., 2019), fault slip rates (Stockmeyer et al., 2017; Peltzer et al., 2020), alluvial sediment provenance (Sawakuchi et al., 2012, 2018; Gray et al., 2019), volcanic eruption ages (Fattahi and

* Department of Earth and Planetary Science, University of California, Berkeley, CA, USA.
E-mail address: nathan.brown@berkeley.edu.

https://doi.org/10.1016/j.geomorph.2020.107296
0169-555X/

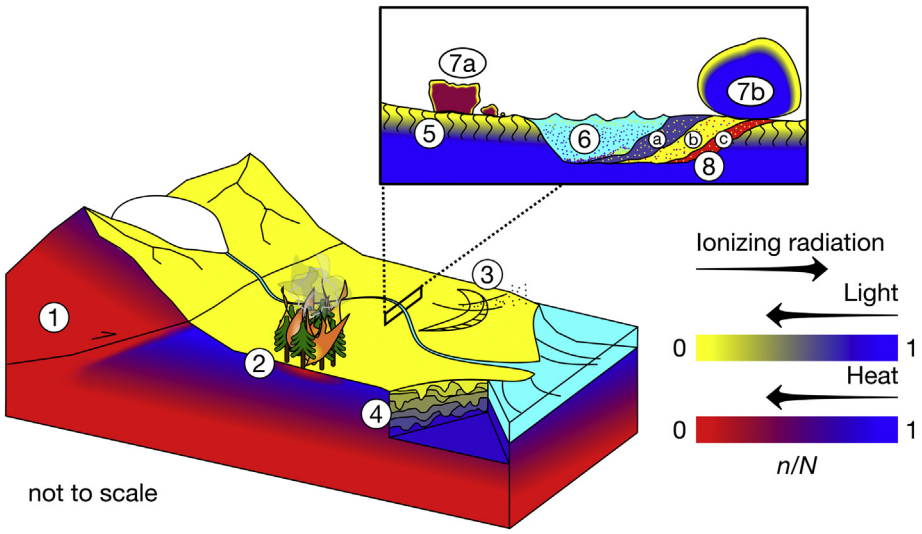

Fig. 1. Luminescence signals slowly accumulate in response to background radiation and deplete with sunlight or heat exposure. Luminescence signals across landscapes therefore contain a wealth of different histories. (1) Tectonic uplift brings rocks to the surface that were recently hot and have not yet reached saturation. (2) Sediments on Earth's surface can also be heated by wildfires or lava flows. The ground surface is covered by grains that are (3) exposed to daily sunlight before eventually (4) being deposited and recording their depositional age. (5) Grains that are mixed into the subsurface encode information about soil mixing. (6) During stream transport, grains very near the water surface may bleach, but grains deeper underwater may remain unexposed to sunlight, retaining a memory of resetting by heat or sunlight exposure long ago. (7) The outer surfaces of cobbles and boulders will progressively bleach to a depth of mm-to-cm, depending on the duration of sunlight exposure and the intensity of rock surface erosion. If the rocks were recently hot (e.g., coming from the uplifting block in location 1), they may retain a thermal signature in their interior (7a), whereas rocks that have long been at atmospheric temperatures will not (7b). (8) Traditional luminescence dating concerns the resetting of grains during transport and before deposition. Such deposits can be poorly bleached (a), well bleached by sunlight (b), or reset by heat (e.g., geothermal heat during exhumation or wildfire exposure) (c).

Stokes, 2003; Preusser et al., 2011; Schmidt et al., 2017b), and others (see Rhodes, 2011; Rittenour, 2018). The present study does not try to describe each of these research fronts in detail, but rather aims to present a simple differential equation and several core principles that unify all of these approaches.

The remainder of this study is divided into four sections. First, a description of how luminescence signals evolve in nature: growing by radiation exposure, reducing by heat exposure and reducing by light exposure. Second, three modelled scenarios to illustrate how complex sample histories are documented by luminescence signals: a sand grain that is exposed to burial, transport, and wildfire; a cobble that is quickly exhumed, exposed to light and submerged in water; and lastly a cobble that experiences internal heating during a wildfire. Third, a general discussion of how different geomorphic processes can be informed by luminescence measurements. Fourth, a note about how the measurement of multiple signals and samples may resolve prior geologic histories that would otherwise be ambiguous.

2. A unified rate equation

Minuscule amounts of energy are constantly accumulating and draining inside common minerals all across Earth's surface. Within an order of magnitude, the build-up rate of this energy is the same. The decay rate, however, varies tremendously. A windblown grain will lose its energy in seconds-to-days, as sunlight releases a signal that may have taken many millennia to collect. By contrast, a grain located several cm from the surface within hard rock may lose and gain its energy at the same pace, the dimmed sunlight competing with background radiation. A deeply buried grain may not lose energy at all. In this case, the grain will reach an upper capacity for energy storage, a limit that may take up to several hundred thousand years to reach (Fig. 2).

To arrive at a unified equation to describe all of these phenomena, I will first briefly describe the differential equations that approximate changes in latent luminescence within grains and cobbles. The net change in luminescence through time is governed by the change in trapped charge (i.e., electrons and electron holes), which usually comprises gain by ionizing radiation, loss by heat exposure, and loss by attenuated and unattenuated sunlight exposure. For a more detailed discussion on luminescence rate equations, see Chen and Pagonis (2011).

2.1. Gain term: Ionizing radiation

Within a deeply buried body of rock, a mineral grain will be impacted by radiation from nearby radioactive isotopes, mostly potassium-40 and the products of uranium and thorium decay chains. Closer to Earth's surface, especially within the upper meter, grains will also absorb radiation from cosmic rays. If a grain were to sit undisturbed, within an unchanging body of sediment or rock, at the same geographic location, it would be bombarded by radiation at an approximately constant rate (Aitken, 1985). Changes in grain size, water content, surrounding sediment radioactivity (e.g., Olley et al., 1996), overburden thickness or density, or even elevation would change this environmental dose rate (Durcan et al., 2015), though typically by less than a factor of two. Most sedimentary quartz and feldspar samples experience geologic dose rates of 1–3 and 3–5 Gy/ka, respectively. K-feldspar grains have a higher concentration of internal radioactivity, mostly from ^{40}K (Huntley and Baril, 1997; Smedley et al., 2012), and therefore generally experience less change in dose rate when they are transported to a new location. This effect is even more pronounced in cobbles, where the dose rate can result almost entirely from within the rock itself (e.g., 93%; Jenkins et al., 2018).

The incoming radiation ionizes the target mineral, generating excited free electrons. This happens continuously in nature. Some of these excited electrons fall into traps before they relax, retaining a small bit of excess energy. The concentration of occupied electron traps n (m^{-3}) begins to grow in proportion to the dose rate (Gy/ka). The number of traps within a crystal lattice N (m^{-3}) is finite however, and after some dose D_0 (Gy) the trap population begins to show saturation effects, filling progressively slower until saturation is complete ($n/N = 1$), despite the ongoing production of free electrons. According to this logic, the electron trapping rate (i.e., the growth in latent luminescence) can be expressed as a single saturating exponential:

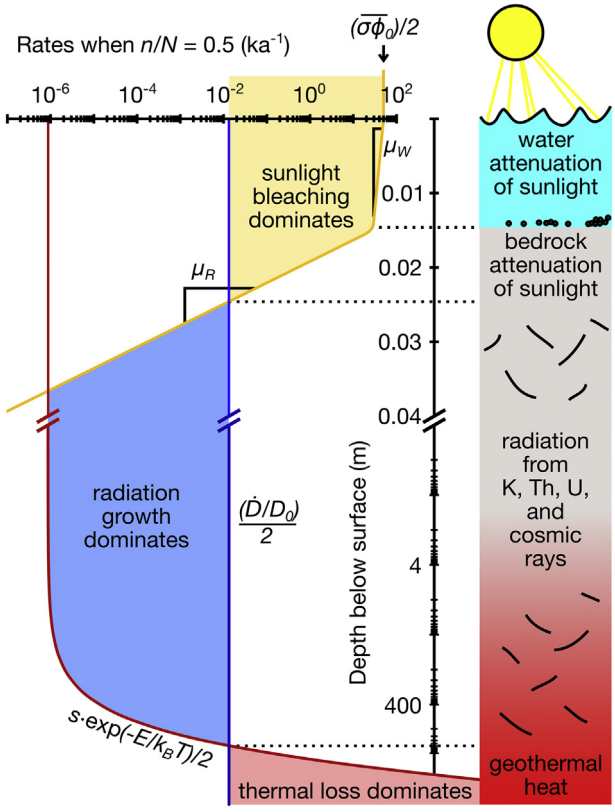

Fig. 2. Rates of trapping (blue line) and detrapping by sunlight (yellow curve) and heat (red curve) are shown for an environment where sunlight is first attenuated by 1.5 cm of water and then by bedrock. These rates will be dependent on the fractional saturation (Eq. (6)). By showing rates when traps are half full, we observe the depths at which different rates are dominant. Below about 2.5 cm depth, bleaching becomes slower than radiation growth and traps will experience net growth. At depths slightly greater than 1.5 km, thermal loss becomes faster than radiation growth and traps will remain mostly and then entirely empty at increasing depths.

$$\frac{d}{dt}\left(\frac{n}{N}\right) = \frac{\dot{D}}{D_0}\left(1-\frac{n}{N}\right) \tag{1}$$

This and alternate expressions have been recently summarized by Guralnik et al. (2015c). Because luminescence ages are calculated assuming no loss since resetting, this equation also implies the apparent age t_{app} (ka) at any fractional saturation value:

$$t_{app} = -\frac{D_0}{\dot{D}}\ln\left(1-\frac{n}{N}\right) \tag{2}$$

A caveat to this idea is that a markedly different dose rate (e.g., by orders of magnitude) may result in a different value of N if the traps are thermally unstable over geologic timescales (Christodoulides et al., 1971). Put differently, the maximum number of traps which can fill at laboratory dose rates (order 10^{-1} Gy/s) can be much higher than those traps which fill at geologic dose rates (order $10^0 - 10^1$ Gy/ka). In feldspar, this is known to be the case (Wintle, 1973; Lamothe et al., 2003). Therefore, workers have developed two distinct concepts: field saturation and laboratory saturation (Kars et al., 2008). For the present study, because I am interested in how luminescence accumulates and depletes naturally (and not how these natural signals might be converted to quantitative histories by comparison with laboratory measurements), I only consider field saturation. I therefore neglect the problem of 'anomalous fading' in feldspars (Huntley and Lamothe, 2001), which would require a more sophisticated approach (Kars et al., 2008).

2.2. Loss term: Heat

In both quartz and feldspar, trapped electrons can be thermally released back to their original lower energies. Quartz OSL obeys first-order kinetics (Bailey, 2001, 2004) and the thermal detrapping rate is expressed in terms of the thermal activation energy, or trap depth, E (eV) and a frequency factor s (s^{-1}):

$$\frac{d}{dt}\left(\frac{n}{N}\right) = -\frac{n}{N}\cdot s\,\exp(-E/k_BT) \tag{3}$$

where k_B is the Boltzmann constant, 8.617×10^{-5} eV/K and T (K) is the absolute temperature of the grain through time (Randall and Wilkins, 1945; Herman et al., 2010).

Feldspars have more complicated kinetics (Jain and Ankjaergaard, 2011; Jain et al., 2015) and workers have developed a number of expressions to relate laboratory and geologic dose-rate and heating responses (Morthekai et al., 2012; Li and Li, 2013; King et al., 2016c; Brown et al., 2017; Brown and Rhodes, 2019; Pagonis and Brown, 2019). For the present study though, I adopt the elegant approach of Jain et al. (2012), and treat feldspar luminescence as thermally activated recombination from within the trap, rather than involving more complicated pathways such as band-tail diffusion. This approximation suits the present task of modelling geologic rates of luminescence loss for the simple reason that charge is likely to be thermally emptied via localized recombination before receiving enough thermal assistance to access the band-tail states (Jain and Ankjaergaard, 2011; Morthekai et al., 2012). Therefore, I approximate thermal loss of feldspar luminescence as analogous to that of quartz (Eq. (3)).

2.3. Loss term: Sunlight

An average photon of sunlight passes entirely through a sand grain (Sohbati et al., 2011). For grains larger than about a mm in diameter, however, or for grains covered by water, the attenuation of sunlight is important. Sunlight reaching Earth's surface comprises many wavelengths, each of which interacts with a trapped electron population with different efficiency. To make matters more complicated, the absorption characteristics of water will depend on turbulence and suspended load (Kirk, 1994; Gray et al., 2017), and in rock, absorption will depend on bulk lithology as well as the opacity of individual grains, including grain shadowing effects (Meyer et al., 2018; Ou et al., 2018; Sellwood et al., 2019). The degree to which sunlight attenuates and changes spectrum throughout natural media like rock and streams is an area of vivid interest for luminescence workers today.

To describe sunlight attenuation in rock and in water, researchers have used the Beer-Lambert law to describe the transmittance of sunlight as exponentially decreasing with depth d (mm) according to some attenuation constant μ (mm^{-1}) and scattering effects, which are not yet well characterized (Sohbati et al., 2011; Gray and Mahan, 2015). To determine the detrapping rate without attenuation from first principles, the radiant flux at every wavelength $\phi(\lambda)$ (m^{-3} s^{-1}) is multiplied by the optical cross-section of the relevant electron trap at that wavelength $\sigma(\lambda)$ (Sohbati et al., 2011). In practice though, workers have adopted a simplified empirical approach by assuming that the attenuation in detrapping can be summarized with two parameters: the detrapping rate at the surface (ka^{-1}) and the attenuation coefficient of the bulk material, μ (mm^{-1}). The final rate equation for sunlight detrapping with attenuation then becomes

$$\frac{\partial}{\partial t}\left(\frac{n}{N}\right) = -\frac{n}{N}\cdot\overline{\sigma\phi}_0\,\exp(-\mu d) \tag{4}$$

This approach requires a site-specific, known-age sample for calibration of the two best-fit parameters. This has been done for several studies involving bedrock (Sohbati et al., 2012; Sohbati et al., 2018; Gliganic et al., 2019). Gray et al. (2017, 2018) have analyzed video footage of

flood waters from the Mojave River to visually estimate sunlight attenuation in comparison to lamp light attenuation in a laboratory water column. Workers have also examined how sediments bleach as they move down rivers (Stokes et al., 2001; Summa-Nelson and Rittenour, 2012; McGuire and Rhodes, 2015a, 2015b; Gray et al., 2018), with all the natural variability in flow conditions, sediment mixing, and so on.

If we assume that, without attenuation, samples will bleach with direct sunlight exposure at a constant rate, , and that this rate decreases only due to the attenuation of light, then the total detrapping rate due to solar bleaching becomes

$$\frac{\partial}{\partial t}\left(\frac{n}{N}\right) = -\frac{n}{N}\cdot\overline{\sigma\phi}_0\ \exp(-\mu_W d_W - \mu_R d_R) \tag{5}$$

where μ_W and mu_R are the attenuation coefficients for water and rock (mm^{-1}), and d_W and d_R are the overburden depths (mm) of each. This approach implies that grains would bleach at a rate of ka^{-1}. As Ou et al. (2018) recently noted in comparison with the dataset of Colarossi et al. (2015), the surficial slices of rocks tend to bleach slower than grains. Likewise, when this parameter is tuned to fit the feldspar grain IRSL natural sunlight bleaching data of Gray et al. (2018), a rate of about 6×10^7 ka^{-1} results, a much higher value than those found when workers fit the expression of Sohbati et al. (2012) to bleaching depth profiles in bedrock surfaces with independent age control (e.g., 4×10^2 - 1×10^5 ka^{-1}; Lehmann et al., 2018; Sohbati et al., 2018). For the purpose of illustrating how sunlight bleaching manifests across a landscape, however, this difference matters little and results in a very slightly deeper bleaching profile in bedrock. Because the timescale of feldspar or quartz grains bleaching in sunlight fundamentally limits whether individual transport events affect the luminescence signals in grains (unlike bedrock bleaching profiles, which are used to calculate total exposure ages or erosion rates integrated over centuries or millennia), I adjust the values of to approximate grain bleaching data (Godfrey-Smith et al., 1988; Gray et al., 2018), not from bedrock surface bleaching data (see Fig. S1).

2.4. Final equation, parameter values, and code availability

Eqs. (1), (3), and (5) combine to give the final result, an equation which describes how the fractional saturation value n/N, re-written here as θ, changes through time in response to changes in light and heat exposure:

$$\frac{\partial\theta}{\partial t} = \frac{D}{D_0}(1-\theta) - \theta\cdot s\ \exp(-E/k_B T) - \theta\cdot\overline{\sigma\phi}_0\ \exp(-\mu_W d_W - \mu_R d_R) \tag{6}$$

Reasonable values for the individual parameters are listed in Table 1. To illustrate possible implementations of this code, a set of MATLAB functions are available online at https://github.com/csdms-contrib/LuSS. As a caveat, this equation is well suited to describe luminescence behavior in a wide range of geomorphic scenarios to a first-order approximation, but is general and heuristic in nature and not intended for the calculation of actual sample histories. For formulations suited to thermochronology and photochronometry applications, see Guralnik and Sohbati (2019).

In the following section, I will give three examples of how this rate equation behaves in diverse grain and cobble transport histories, using the provided functions and assuming the values listed in Table 1. Section 4 will then use this equation to systematically explore how various geomorphic processes influence luminescence signals.

3. Examples of simulated geologic histories

3.1. Example 1: Quartz grain wandering through a landscape

Fig. 3 shows how the luminescence signal from a quartz grain might change during its lifetime. Before the grain is exposed at the surface, and in the absence of rapid bedrock cooling or other thermal disturbance (e.g., wildfire), all electron traps will be full (Fig. 3a). Within the first several seconds of sunlight exposure, however, all of the relevant OSL traps will empty (Fig. 3b). Next, this grain is buried by a constant supply of sand, accumulating up to 10 cm over 10 ka. Initially, sunlight will still filter through the thin layer of overburden grains, but eventually the sediment will thicken into an opaque cover and the geologic trapping rate will exceed any amount of optical or thermal detrapping. In Fig. 3c, this crossover happens when the sediment is a few cm thick (the thickness at which sunlight bleaching is negligible will be primarily controlled by the effective rock attenuation coefficient for the sediment, μ_R, and to a lesser extent, the detrapping rate constant,). After 20 ka of burial, the grain is transported by stream for 12 h with a water column thickness of 20 cm. Due to the rapid bleaching rate of the quartz OSL signal, the accumulated burial signal is bleached within a few hours (Fig. 3d). This transport event is followed by another burial period of 30 ka, during which nearly 40% of the traps fill (Fig. 3e) before the sample is heated during a wildfire (Fig. 3f). Over a period of 2 h, the grain reaches a peak temperature of 500 °C and all of the accumulated signal is lost due to heating. The grain then rests for another 5 ka before collection (Fig. 3g).

If this grain were dated, the geomorphologist would measure an apparent age of 5 ka (Eq. (2)). Interpreted as the time since resetting, either by heat or light, this age would be correct. Of course, often an OSL age is assumed to represent the time since *sunlight* exposure, which, in our example, would be incorrect.

3.2. Example 2: Feldspar within a clast eroding from an active orogen

The second example involves bedrock which rapidly cools ($dT/dt = -1$ °C/ka) for 100 ka as it exhumes up through the crust to Earth's surface, where it erodes out to become a clast of radius 3 cm (Fig. 4a). Upon reaching the surface, the clast is in thermal disequilibrium with the atmosphere, meaning that the trapping rate within the dark interior of the clast is significantly greater than the thermal detrapping rate at surficial temperatures. Left to sit for several hundred thousand years, the clast would

Table 1
Parameter values used in this study.

Symbol	Units	Description	Quartz	K-feldspar
θ	dimensionless	Fraction of field saturation	History dependent	
	$Gy\cdot ka^{-1}$	Geologic dose rate	2	4
D_0	Gy	Characteristic dose of saturation	150	225
s	s^{-1}	Trap frequency factor	2.8×10^{12}	1×10^{14}
E	eV	Trap activation energy	1.59	1.70
	ka^{-1}	Unattenuated detrapping rate at ground level	1.05×10^{10}	6.10×10^7
μ_R	mm^{-1}	Attenuation coefficient in rock	0.5	1.0
μ_W	mm^{-1}	Attenuation coefficient in water	0.034	
d_W, d_R	mm	Attenuation depth in water or rock	History dependent	

[1]Literature values include E and s values from Spooner and Questiaux (2000) (quartz) and Murray et al. (2009) (K-feldspar); values adopted from datasets of Colarossi et al. (2015) (quartz) and Gray et al. (2018) (K-feldspar); μ_W value from Gray et al. (2018).

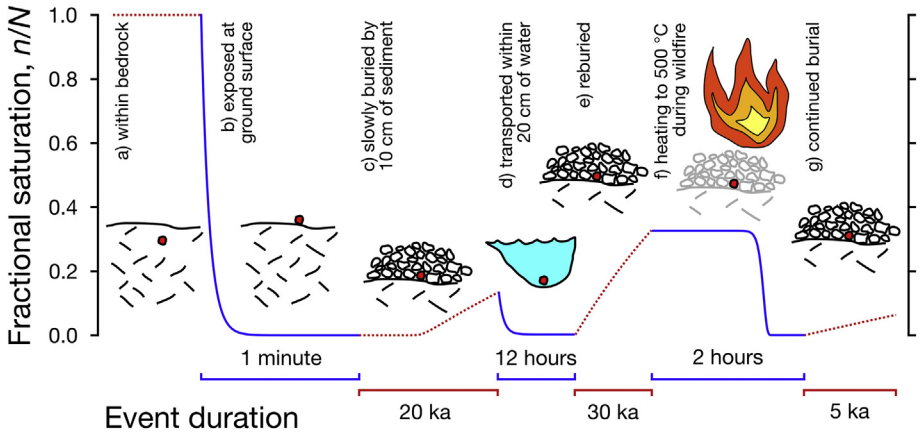

Fig. 3. An imaginary history of trap filling and emptying is shown for a quartz grain governed by Eq. (6). Notice the changing timescales.

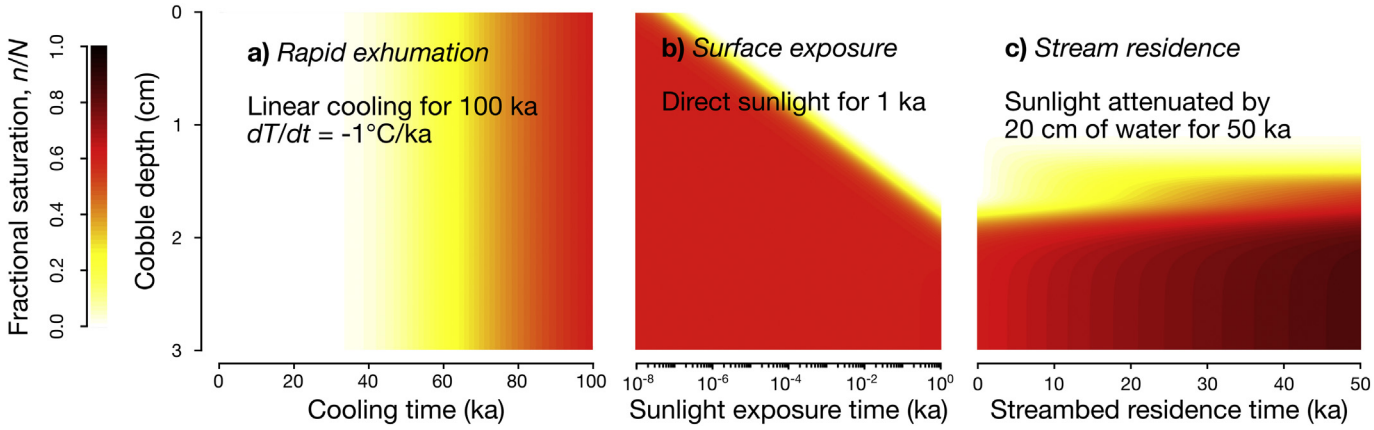

Fig. 4. Feldspar fractional saturation is shown for a clast of radius 3 cm during a history of (a) exhumation, (b) exposure to direct sunlight (notice the logarithmic time axis for this panel), and (c) exposure to sunlight attenuated by 20 cm of water. See also Fig. 5, which shows the n/N depth-profile at the end of each phase.

eventually reach equilibrium ('field saturation'; Kars et al., 2008). Put differently, as the clast erodes out after exhumation, it carries with it a memory of its recent thermal history.

At the surface, this clast is exposed to direct sunlight for 1 ka. This sunlight exposure causes a solar bleaching front to migrate into the clast interior logarithmically through time (Fig. 4). As with the thermal disequilibrium, the clast is in optical disequilibrium and detrapping in response to sunlight will continue until the trapping from internal clast radioactivity equals detrapping from attenuated incoming sunlight. If the surface of the clast is eroded, this equilibrium depth will once again be in disequilibrium. In this way, the equilibrium depth can contain information about clast comminution or bedrock lowering rates (Sohbati et al., 2018).

In Fig. 4, direct sunlight bleaching is interrupted after 1 ka, when the rock is submerged in 20 cm of water for 50 ka. Two interesting things happen during this stream residence time. First, the dark center of the clast continues to experience net trapping, with the n/N value increasing from 0.62 to 0.84. This represents the rock slowly returning to thermal equilibrium. Second, the bleaching front that evolved during the 1 ka of direct sunlight exposure recedes, coming closer to the rock surface. This is shown more clearly in Fig. 5 which illustrates the final n/N depth profile after each of the three phases of clast history. Within the clast, four depth domains exist (Fig. 5). In domain I, all traps remain empty due to the ongoing underwater bleaching. In domain II, traps which were emptied during direct sunlight exposure can now accumulate under reduced lighting conditions. Domain III represents the partially bleached front that developed during direct sunlight exposure. As in domain II, traps in domain III began to refill when the clast was submerged in water. Lastly, domain IV represents the innermost portion of the clast which was never affected by sunlight and has continued to accumulate trapped charge since cooling during exhumation. The age

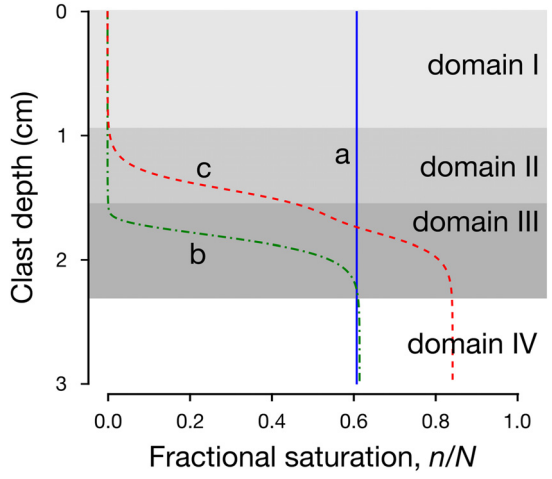

Fig. 5. The fractional saturation depth profile is shown after the (a) exhumation, (b) direct sunlight exposure, and (c) exposure to subaqueous sunlight. The four domains show depths which (I) remain fully bleached due to subaqueous sunlight; (II) fully bleached during subaerial bleaching but have begun to refill despite subaqueous sunlight; (III) partially bleached during direct sunlight exposure and have since begun to refill; (IV) remain unbleached by sunlight. Compare with Fig. 4.

from this portion of the rock would therefore represent the 'cooling age' (Dodson, 1973).

3.3. Example 3: Feldspar within a cobble exposed to wildfire

The third example history involves a cobble of radius 8 cm subjected to a wildfire (Fig. 6). All luminescence traps within the cobble are saturated before the fire. A wildfire is then simulated by modelling the cobble as a sphere with an initial uniform temperature of 10 °C introduced into an infinite heat bath of temperature 400 °C for 20 min (Fig. 6). Heat is exchanged between the rock and air by convection and then conducted into the interior of the cobble according to a one-dimensional solution to the heat equation in spherical coordinates (e.g., p. 303; Bergman et al., 2011) assuming standard thermal parameters for granite: thermal diffusivity of 1.6×10^{-6} m^2/s, thermal conductivity of 2 W/m·K, and convective heat transfer coefficient of 50 W/(m^{2}K) (Butler, 2010).

The detrapping that results produces an interesting saturation-depth relationship. Because some heat penetrates into the center of the cobble (Fig. 6), the fractional saturation within the center of the cobble is lowered to just above 0.9 (Fig. 6d). This final pattern of saturation with depth resulting from wildfire exposure is comparable to the result shown in Figs. 4b and 5b, caused by recent tectonic exhumation and sunlight exposure. Judging only by the luminescence depth profiles of these two rocks, it is impossible to resolve that these cobbles experienced two very different histories. Possible approaches to avoid this ambiguity are mentioned in Section 5.

4. Sensitivity of luminescence signals to different geomorphic processes

The example histories presented so far demonstrate how rocks and sediments may record multiple geomorphic events within a given luminescence signal. But which events matter? Which events fully or partially reset signals and over what timescales?

Fig. 7 illustrates how sensitive luminescence signals are to different geomorphic processes by comparing simulated decay and regeneration timescales (Fig. 7a) with approximate $T - t$ domains for different processes (Fig. 7b). Many of these domains are site-specific. For example, consider the $T - t$ domain shown for fault gouge material (Fig. 7b). The intra-fault temperature during an earthquake will depend upon the magnitude of the earthquake and the frictional properties of the rupturing rock. Likewise, the ambient temperature between earthquakes will depend upon the depth of the sample beneath the surface and the geothermal gradient. As researchers can extract drill core samples that cross faults at a few km below the surface (e.g., Spencer et al., 2012), I drew a long-term temperature window of about 30 to 100 °C. The simulated timescales are calculated for K-feldspar (Fig. 7c) and quartz (Fig. 7d) grains and shown together with the geomorphic domain shapes. For simplicity, this figure applies only to grains; the time required for heat or light diffusion into rock is neglected.

Direct exposure to lava flows is predicted to thermally reset the luminescence signals within K-feldspars and quartz grains. This is consistent with many previous studies of fully reset sediment adjacent to lava flows as well as xenoliths entrained within flows (Forman et al., 1994; Fattahi and Stokes, 2003; Rufer et al., 2012; Rittenour et al., 2012; Schmidt et al., 2017a, 2017b). While OSL signals are predicted to empty

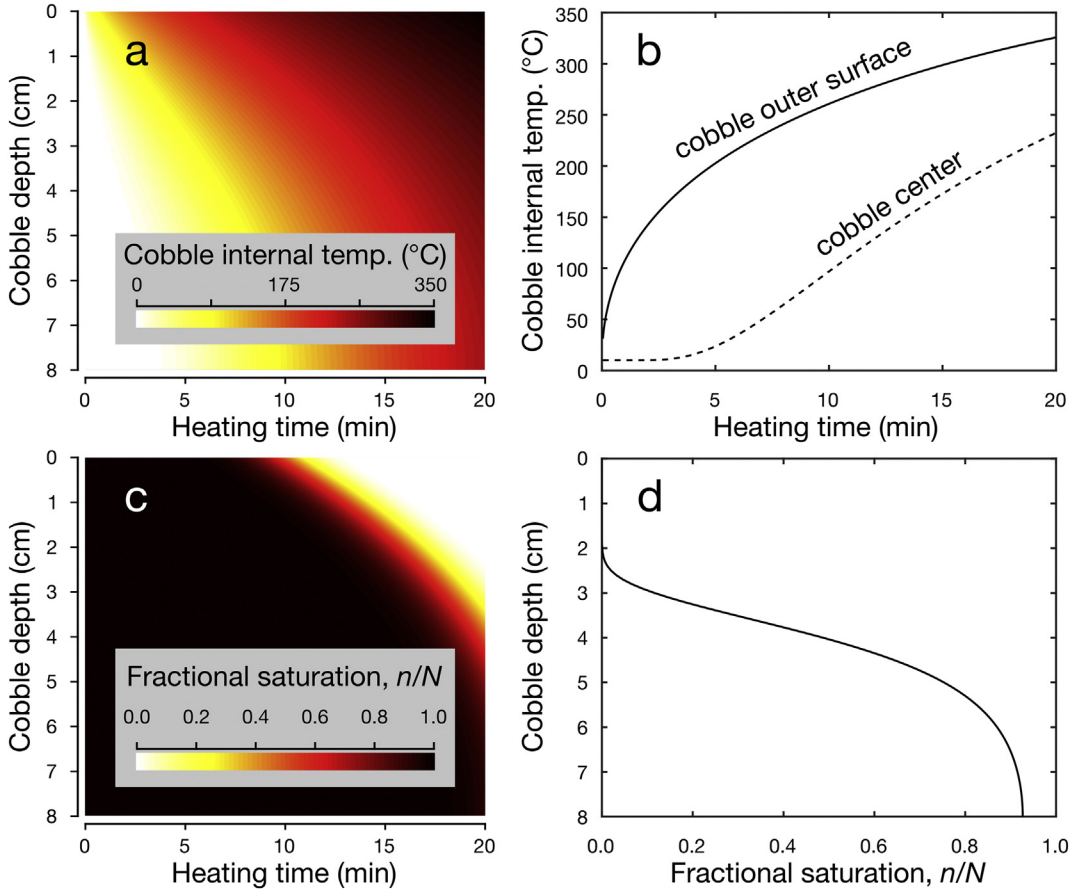

Fig. 6. Feldspar fractional saturation is shown for a cobble of radius 8 cm, exposed to a wildfire at 400 °C for 20 min. (a) Forced by heating at the surface, the interior of the cobble heats by conduction. (b) For short-duration events like this, the outer surface of the cobble experiences a greater temperature change than the center. In this case, this difference is about 100 °C. (c) As the heat penetrates into the cobble, the near-surface traps are entirely emptied, while those closer to the center are reduced to n/N=0.93. (d) The fractional saturation depth-profile is shown after the simulated wildfire. Notice the similar form of (d) with Fig. 5b, despite the very different histories.

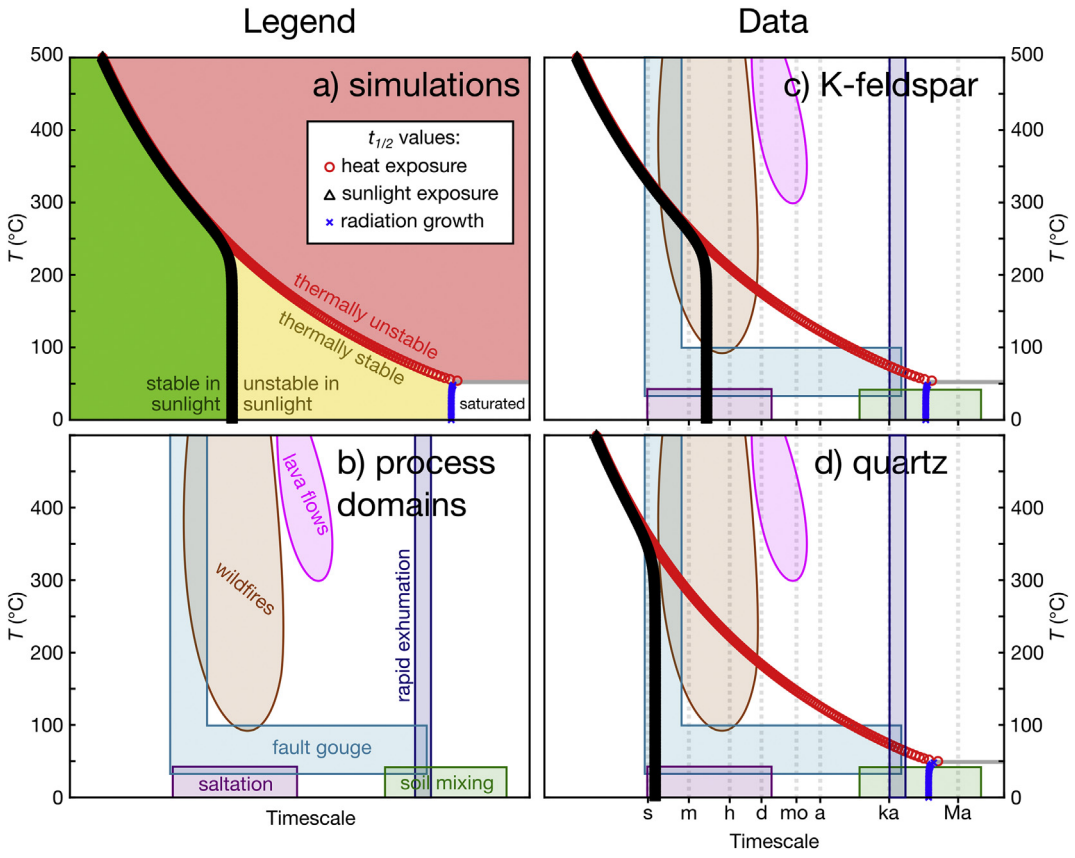

Fig. 7. (a) Simulation results are used to calculate the time required for luminescence signals to deplete from full to half-full in response to heat (red circles) or sunlight (black triangles). The blue *x* symbols show the time required for signals to accumulate from empty to half-full in response to geologic radiation without sunlight as a function of temperature. These values delineate regions which are thermally unstable (red region), thermally stable but unstable in sunlight (yellow region), thermally stable and stable in sunlight (green region), or in field saturation (white region). Notice that at a certain temperature, the signal will remain half-full, as shown with a gray line. (b) Approximate time and temperature domains for relevant geomorphic processes. According to the legends given in (a) and (b), the simulation results for K-feldspar and quartz OSL signals are shown in panels (c) and (d), respectively.

when exposed to any lava flow event, the other geomorphic processes shown in Fig. 7 produce a wider range of signals.

For instance, wildfires produce very different subsurface temperatures within a soil. Depending upon the depth, type of fuel, moisture content and composition of the soil, temperatures may be only slightly elevated, or may reach values in excess of 600 °C (Campbell et al., 1995; Busse et al., 2005). Because the burn time of a wildland fire at a particular location typically ranges from minutes to days, a given fire may or may not thermally empty OSL signals within soils, according to the simulation predictions (Fig. 7c, d). An exposure of 200 °C for a minute would not result in signal resetting, but 300 °C for an hour would. Few studies have directly investigated wildfire effects on luminescence signals, but results from soils within two burn areas indicate that partial luminescence loss does occur after wildfires (Rhodes et al., 2004; Rengers et al., 2017). Moreover, the intensity of heat experienced by a burned soil might be archived within the luminescence signal (Rengers et al., 2017), similar to how burned archaeological material records the maximum thermal exposure (Spencer and Sanderson, 1994).

Whether OSL signals in fault gouge are reset depends both on the earthquake effects as well as the long-term burial temperature of the samples (Banerjee et al., 1999), as illustrated by the 'L' shape of this domain in Fig. 7b. This leads to ambiguity when interpreting signals that are not in saturation, as has been observed in several studies (Singhvi et al., 1994; Mukul et al., 2007; Spencer et al., 2012). Researchers also are unsure how earthquake-related stress effects may reduce luminescence intensity (Ikeya et al., 1982; Banerjee et al., 1999; Porat et al., 2007).

Bedrock that is exhumed to Earth's surface will cool, transitioning from a temperature that depletes the OSL signal to a temperature where the signal begins to accumulate (Guralnik et al., 2015a). This accumulation eventually produces saturation. Prior to saturation, however, the rock will retain an apparent age. If rock is brought to the surface rapidly, it may not yet be saturated. Unfortunately, for most OSL signals, the minimum resolvable cooling rate is quite high (>200 °C/Ma; King et al., 2016a).

To compare the $T - t$ domain of exhumation with the other processes in this section is complicated by the fact that, for exhumation, the temperature of the rock is continuously changing over the timescale of interest. The other processes mentioned so far can be effectively simplified as events where heat exposure at a fixed temperature occurs for a given duration. For the sake of comparison, we show rapid exhumation as the duration of time at a given temperature for linear cooling rates of 200 to 1000 °C/Ma. If we assume that the minimum resolvable geologic temperature difference is on the order of 1 °C (Guralnik et al., 2015b; Brown et al., 2017), then the timescales (i.e., *dt* values) corresponding to these rates are approximately 1 to 5 ka. During rapid cooling, the luminescence system will become thermally stable while still unsaturated. As shown in Fig. 7c and d, there will be a period of time, on the order of 10^2 ka, during which the signal will record the time since reaching the 'closure temperature,' that is, the 'closure age' (Dodson, 1973; Guralnik et al., 2013). After this period of disequilibrium during rapid cooling, the system will reach field saturation and would only be useful for providing minimum cooling ages.

Traditionally, luminescence workers avoid sampling sediment within soil horizons. This is partly because the radioactivity may be in disequilibrium (Olley et al., 1996), but also because grains may reach the ground surface and lose their accumulated luminescence. Because the mixing timescale of soils is much greater than the time necessary to bleach quartz

or feldspar luminescence signals, any grain that is advected to the ground surface will be completely bleached and will no longer yield a depositional age (e.g., Porat et al., 2018). Once the grain is reburied into the soil, however, it will yield an age that relates to mixing characteristics and not to the original deposition (Stang et al., 2012; Reimann et al., 2017; Furbish et al., 2018a; Gray et al., 2020). The soil residence time may be so great that many grains that were reincorporated into the soil will have since reached signal saturation and will no longer record the travel time from the surface (Furbish et al., 2018a). However, in many natural datasets, luminescence signals from soil profiles are below saturation reflecting a mixing timescale less than the saturation timescale (Reimann et al., 2017; Román-Sánchez et al., 2019a, 2019b; Gray et al., 2020).

Unlike with soil mixing timescales, grain exposure during subaerial transport (e.g., saltation) can be so brief (Martin et al., 2013) that K-feldspar luminescence signals are not entirely bleached. For this reason, geomorphologists must be certain of sufficient sunlight exposure prior to burial. With quartz grains, complete bleaching occurs within seconds and virtually all windblown quartz transported in full daylight will be completely reset before burial (Godfrey-Smith et al., 1988; Colarossi et al., 2015). A comparison of Fig. 7c and d illustrates this point: the timescale for K-feldspar bleaching is comparable to the timescale of saltation, whereas the quartz OSL signal will be totally bleached during saltation.

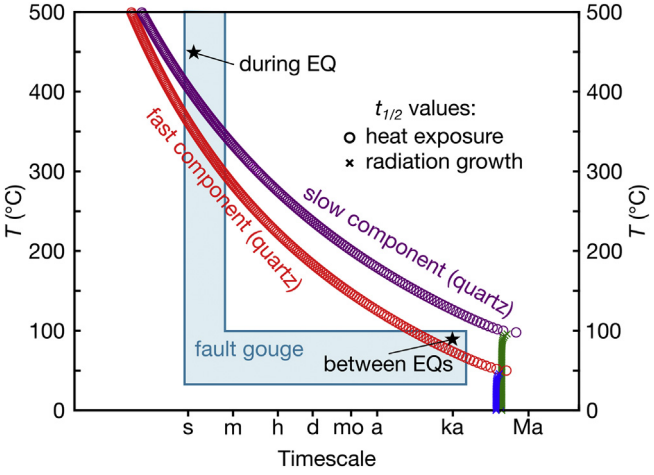

Fig. 8. A comparison of thermal stability between the fast and slow component signals in quartz. An imaginary quartz grain within fault gouge sits at an ambient temperature of 90 °C between earthquakes and reaches 450 °C for a few seconds during each earthquake (two black stars on figure). In this example, the fast component signal would be reset by the ambient geologic temperature between earthquakes, but the slow component signal would only be reset during earthquakes. In this way, the fast component would give information about burial temperature and the slow component would give information about the earthquake recurrence interval.

5. Leveraging multiple signals to understand a sample's history

The luminescence signals mentioned so far, the OSL fast component in quartz and the low-temperature IRSL signal in K-feldspar, are commonly measured, but a variety of other signals can be readily obtained (Krbetschek et al., 1997). In quartz, these signals are discrete and vary in thermal and optical stability (Preusser et al., 2009). In feldspars, signals vary in optical and thermal stability (Duller, 1997), but often within a continuum (Visocekas et al., 1994; Thomsen et al., 2008; Li and Li, 2011). The number of luminescence signals that can be measured from a single sample will vary according to the natural properties of the sample (Visocekas et al., 1994; Krbetschek et al., 1997; Guralnik et al., 2015a), but users can significantly improve their power to interpret a sample's history by measuring several luminescence signals with different sensitivity to sunlight or heat (e.g., McGuire and Rhodes, 2015a, 2015b; Reimann et al., 2015; King et al., 2016c). This is analogous to how workers routinely measure multiple cosmogenic radionuclides to better constrain burial histories (Reiners et al., 2005) or multiple thermochronometric systems to resolve cooling histories (Granger, 2006).

As an example, Fig. 8 compares the thermal stability of the fast and slow component signals of quartz by plotting the time required to half-way empty both signals at a range of temperatures (shown as red and purple circles). Also shown as green and blue *x* symbols are the times required to half-way fill both signals. The two black stars in Fig. 8 represent an imaginary fault gouge sample that rests at an ambient temperature of 90 °C for 1 ka before rupturing and undergoing shear heating to 450 °C for several seconds. In this example, the fast component signal from this sample would be depleted by the ambient geothermal heat and could only be used to infer some minimum burial temperature. The slow component, however, would be thermally reset only during earthquake events and would therefore yield an age since the last earthquake. As both feldspar and quartz contain multiple luminescence signals ranging in thermal and optical stability, the strategy of measuring multiple signals to rule out potential geologic histories is promising.

Finally, it is important to note that, while this study has focused on luminescence signals evolving within individual grains or rocks, in practice, researchers routinely measure multiple grains, aliquots, cobbles and samples to properly characterize a population. For example, a minority of grains may still yield an accurate depositional age for a sediment package that was incompletely exposed to sunlight (Galbraith et al., 1999). By measuring many grains, aliquots, cobbles or samples and then applying appropriate statistical models (Galbraith and Roberts, 2012), workers can resolve past environmental conditions more completely.

6. Conclusion

The model presented in this study and the simulations performed demonstrate how luminescence signals within individual grains, cobbles, and bedrock surfaces archive abundant information. Wildfires, geothermal heating or cooling histories, subaerial or subaqueous transport events, bedrock exposure to sunlight and long-term rock surface lowering rates can all affect the luminescence signals within common minerals like quartz and feldspar. While there has been much work recently to describe these phenomena separately, it remains important to remember that a given mineral may have experienced several different exposures to heat or light during the past several hundred thousand years. By evaluating the sensitivity of luminescence signals to a wide range of geomorphic phenomena, we can estimate which events may be recorded within a sample. The numerical results contained here are therefore encouraging and cautionary. Encouraging in that multiple events might be extracted from a single rock, and cautionary in that the geomorphologist might misinterpret the number or nature of these events. By considering various sources of heat and sunlight that a sample may have experienced (e.g., Fig. 7), by measuring multiple luminescence signals with different sensitivities to heat and sunlight, and by applying proper summary statistics to measurements of multiple targets (e.g., grains, aliquots, cobbles), users can improve their resolution of a sample's recent history and minimize the risk of misinterpretation.

Declaration of competing interest

The authors declare that they have no known competing financial interests or personal relationships that could have appeared to influence the work reported in this paper.

Acknowledgements

I would like to thank reviewers Arjun Heimsath, Harrison Gray, and Jakob Wallinga for their constructive comments which have significantly improved this study. My work is supported by NSF award number 1806629.

Appendix A. Supplementary data

Supplementary data to this article can be found online at https://doi.org/10.1016/j.geomorph.2020.107296.

References

Aitken, M., 1985. Thermoluminescence Dating. Academic Press, London.

Bailey, R.M., 2001. Towards a general kinetic model for optically and thermally stimulated luminescence of quartz. Radiat. Meas. 33, 17–45.

Bailey, R.M., 2004. Paper I - simulation of dose absorption in quartz over geological timescales and its implications for the precision and accuracy of optical dating. Radiat. Meas. 38, 299–310.

Balescu, S., Ritz, J.F., Lamothe, M., Auclair, M., Todbileg, M., 2007. Luminescence dating of a gigantic palaeolandslide in the Gobi-Altay mountains, Mongolia. Quat. Geochronol. 2, 290–295.

Banerjee, D., Singhvi, A.K., Pande, K., Gogte, V.D., Chandra, B.P., 1999. Towards a direct dating of fault gouges using luminescence dating techniques: Methodological aspects. Curr. Sci. 77, 256–268.

Bergman, T.L., Lavine, A.S., Incropera, F.P., DeWitt, D.P., 2011. Introduction to Heat Transfer. Wiley (Sixth edition).

Biswas, R.H., Herman, F., King, G.E., Braun, J., 2018. Thermoluminescence of feldspar as a multi-thermochronometer to constrain the temporal variation of rock exhumation in the recent past. Earth Planet. Sci. Lett. 495, 56–68.

Bristow, C.S., Augustinus, P.C., Wallis, I.C., Jol, H.M., Rhodes, E.J., 2010. Investigation of the age and migration of reversing dunes in Antarctica using GPR and OSL, with implications for GPR on Mars. Earth Planet. Sci. Lett. 289, 30–42.

Brown, N.D., Moon, S., 2019. Revisiting erosion rate estimates from luminescence profiles in exposed bedrock surfaces using stochastic erosion simulations. Earth Planet. Sci. Lett. 528, 115842.

Brown, N.D., Rhodes, E.J., 2017. Thermoluminescence measurements of trap depth in alkali feldspars extracted from bedrock samples. Radiat. Meas. 96, 53–61.

Brown, N.D., Rhodes, E.J., 2019. Dose-rate dependence of natural TL signals from feldspars extracted from bedrock samples. Radiat. Meas. 128, 106188.

Brown, N., Rhodes, E., Antinao, J.L., McDonald, E., 2015. Single-grain post-IR IRSL signals of K-feldspars from alluvial fan deposits in Baja California Sur, Mexico. Quat. Int. 362, 132–138.

Brown, N.D., Rhodes, E.J., Harrison, T.M., 2017. Using thermoluminescence signals from feldspars for low-temperature thermochronology. Quat. Geochronol. 42, 31–41.

Busse, M.D., Hubbert, K.R., Fiddler, G.O., Shestak, C.J., Powers, R.F., 2005. Lethal soil temperatures during burning of masticated forest residues. Int. J. Wildland Fire 14, 267–276.

Butler, B.W., 2010. Characterization of convective heating in full scale wildland fires. In: Viegas, D.X. (Ed.), VI International Conference on Forest Fire Research.

Campbell, G.S., Jungbauer, J.D., Bristow, K.L., Hungerford, R.D., 1995. Soil temperature and water content beneath a surface fire. Soil Sci. 159, 363–374.

Chamberlain, E.L., Wallinga, J., Reimann Jr., T., S.L.G., Streckler, M.S., Shen, Z., Sincavage, R., 2017. Luminescence dating of delta sediments: novel approaches explored for the Ganges-Brahmaputra-Meghna Delta. Quat. Geochronol. 41, 97–111.

Chamberlain, E.L., Tornqvist, T.E., Shen, Z., Mauz, B., Wallinga, J., 2018. Anatomy of Mississippi Delta growth and its implications for coastal restoration. Sci. Adv. 4, 1–9.

Chamberlain, E.L., Mehta, J.M., Reimann, T., Wallinga, J., 2020. A geoarcharological perspective on the challenges and trajectories of Mississippi Delta communities. Geomorphology 360, 107132.

Chen, R., Pagonis, V., 2011. Thermally and Optically Stimulated Luminescence: A Simulation Approach. Wiley.

Christodoulides, C., Ettinger, K.V., Fremlin, J.H., 1971. The use of TL glow peaks at equilibrium in the examination of the thermal and radiation history of minerals. Mod. Geol. 2, 275–280.

Colarossi, D., Duller, G.A.T., Roberts, H.M., Tooth, S., Lyons, R., 2015. Comparison of paired OSL and feldspar post-IR IRSL dose distributions in poorly bleached fluvial sediments from South Africa. Quat. Geochronol. 30, 233–238.

Del Vecchio, J., Lang, K.A., Robins, C.R., McGuire, C.P., Rhodes, E.J., 2018. Storage and weathering of landslide debris in the eastern San Gabriel Mountains, California, USA: implications for mountain solute flux. Earth Surf. Process. Landf. 43, 2724–2737.

Dodson, M., 1973. Closure temperature in cooling geochronological and petrological systems. Contrib. Mineral. Petrol. 40, 259–279.

Duller, G.A.T., 1997. Behavioural studies of stimulated luminescence from feldspars. Radiat. Meas. 27, 663–694.

Durcan, J.A., King, G.E., Duller, G.A.T., 2015. DRAC: Dose Rate and Age Calculator for trapped charge dating. Quat. Geochronol. 28, 54–61.

Fattahi, M., Stokes, S., 2003. Dating volcanic and related sediments by luminescence methods: a review. Earth Sci. Rev. 62, 229–264.

Forman, S.L., Pierson, J., Smith, R.P., Hackett, W.R., Valentine, G., 1994. Assessing the accuracy of thermoluminescence for dating baked sediments beneath late Quaternary lava flows, Snake River Plain, Idaho. J. Geophys. Res. 99, 15569–15576.

Freiesleben, T., Sohbati, R., Murray, A., Jain, M., al Khasawneh, S., Hvidt, S., Jakobsen, B., 2015. Mathematical model quantifies multiple daylight exposure and burial events for rock surfaces using luminescence dating. Radiat. Meas. 81, 16–22.

Fujioka, T., Chappell, J., Fifield, L.K., Rhodes, E.J., 2009. Australian desert dune fields initiated with Pliocene-Pleistocene global climatic shift. Geology 37, 51–54.

Fuller, T.K., Perg, L.A., Willenbring, J.K., Lepper, K., 2009. Field evidence for climate-driven changes in sediment supply leading to strath terrace formation. Geology 37, 467–470.

Furbish, D.J., Roering, J.J., Almond, P., Doane, T.H., 2018a. Soil particle transport and mixing near a hillslope crest: 1. Particle ages and residence times. J. Geophys. Res. Earth Surf. 123, 1052–1077.

Furbish, D.J., Roering, J.J., Keen-Zeebert, A., Almond, P., Doane, T.H., Schumer, R., 2018b. Soil particle transport and mixing near a hillslope crest: 2. Cosmogenic nuclide and optically stimulated luminescence tracers. J. Geophys. Res. Earth Surf. 123, 1078–1093.

Galbraith, R.F., Roberts, R.G., 2012. Statistical aspects of equivalent dose and error calculation and display in OSL dating: an overview and some recommendations. Quat. Geochronol. 11, 1–27.

Galbraith, R.F., Roberts, R.G., Laslett, G.M., Yoshida, H., Olley, J.M., 1999. Optical dating of single and multiple grains of quartz from Jinmium rock shelter, northern Australia: part i, experimental design and statistical models. Archaeometry 41, 339–364.

Gliganic, L.A., Meyer, M.C., Sohbati, R., Jain, M., Barrett, S., 2019. OSL surface exposure dating of a lithic quarry in Tibet: laboratory validation and application. Quat. Geochronol. 49, 199–204.

Godfrey-Smith, D.I., Huntley, D.J., Chen, W.H., 1988. Optical dating studies of quartz and feldspar sediment extracts. Quat. Sci. Rev. 7, 373–380.

Granger, D.E., 2006. A review of burial dating methods using ^{26}Al and ^{10}Be. Geol. Soc. Am. Spec. Pap. 415, 1–16.

Gray, H.J., Mahan, S.A., 2015. Variables and potential models for the bleaching of luminescence signals in fluvial environments. Quat. Int. 362, 42–49.

Gray, H.J., Tucker, G.E., Mahan, S.A., McGuire, C., Rhodes, E.J., 2017. On extracting sediment transport information from measurements of luminescence in river sediment. J. Geophys. Res. Earth Surf. 122, 654–677.

Gray, H.J., Tucker, G.E., Mahan, S.A., 2018. Application of a luminescence-based sediment transport model. Geophys. Res. Lett. 45, 6071–6080.

Gray, H.J., Jain, M., Sawakuchi, A.O., Mahan, S.A., Tucker, G.E., 2019. Luminescence as a sediment tracer and provenance tool. Rev. Geophys. 57, 987–1017.

Gray, H.J., Keen-Zebert, A., Furbish, D.J., Tucker, G.E., Mahan, S.A., 2020. Depth-dependent soil mixing persists across climate zones. Proc. Natl. Acad. Sci. U. S. A. 117, 8750–8756.

Guralnik, B., Sohbati, R., 2019. Advances in physics and applications of optically and thermally stimulated luminescence. World Scientific. Chapter Fundamentals of Luminescence Photo- and Thermochronometry, pp. 399–437.

Guralnik, B., Jain, M., Herman, F., Paris, R.B., Harrison, T.M., Murray, A.S., Valla, P.G., Rhodes, E.J., 2013. Effective closure temperature in leaky and/or saturating thermochronometers. Earth Planet. Sci. Lett. 384, 209–218.

Guralnik, B., Ankjaergaard, C., Jain, M., Murray, A.S., Muller, A., Walle, M., Lowick, S., Preusser, F., Rhodes, E.J., Wu, T.S., Mathew, G., Herman, F., 2015a. OSL-thermochronometry using bedrock quartz: a note of caution. Quat. Geochronol. 25, 37–48.

Guralnik, B., Jain, M., Herman, F., Ankjaergaard, C., Murray, A.S., Valla, P.G., Preusser, F., King, G. E., Chen, R., Lowick, S.E., Kook, M., Rhodes, E.J., 2015b. OSL-thermochronometry of feldspar from the KTB borehole, Germany. Earth Planet. Sci. Lett. 423, 232–243.

Guralnik, B., Li, B., Jain, M., Chen, R., Paris, R.B., Murray, A.S., Li, S.H., Pagonis, V., Valla, P.G., Herman, F., 2015c. Radiation-induced growth and isothermal decay of infrared-stimulated luminescence from feldspar. Radiat. Meas. 81, 224–231.

Heimsath, A.M., Chappell, J., Spooner, N.A., Questiaux, D.G., 2002. Creeping soil. Geology 30, 111–114.

Herman, F., Rhodes, E.J., Braun, J., Heiniger, L., 2010. Uniform erosion rates and relief amplitude during glacial cycles in the Southern Alps of New Zealand, as revealed from OSL-thermochronology. Earth Planet. Sci. Lett. 297, 183–189.

Hesse, P.P., 2016. How do longitudinal dunes respond to climate forcing? Insights from 25 years of luminescence dating of the Australian desert dunefields. Quat. Int. 410, 11–29.

Huntley, D.J., Baril, M.R., 1997. The K content of the K-feldspars being measured in optical dating or in thermoluminescence dating. Ancient TL 15, 11–13.

Huntley, D.J., Lamothe, M., 2001. Ubiquity of anomalous fading in K-feldspars and the measurement and correction for it in optical dating. Can. J. Earth Sci. 38, 1093–1106.

Ikeya, M., Miki, T., Tanaka, K., 1982. Dating of a fault by electron spin resonance on intrafault materials. Science 215, 1392–1393.

Jain, M., Ankjaergaard, C., 2011. Towards a non-fading signal in feldspar: insight into charge transport and tunnelling from time-resolved optically stimulated luminescence. Radiat. Meas. 46, 292–309.

Jain, M., Guralnik, B., Andersen, M.T., 2012. Stimulated luminescence emission from localized recombination in randomly distributed defects. J. Phys. Condens. Matter 24, 385402.

Jain, M., Sohbati, R., Guralnik, B., Murray, A.S., Kook, M., Lapp, T., Prasad, A.K., Thomsen, K. J., Buylaert, J.P., 2015. Kinetics of infrared stimulated luminescence from feldspars. Radiat. Meas. 81, 242–250.

Jenkins, G.T.H., Duller, G.A.T., Roberts, H.M., Chiverrell, R.C., Glasser, N.F., 2018. A new approach for luminescence dating glaciofluvial deposits – high precision optical dating of cobbles. Quat. Sci. Rev. 192, 263–273.

Johnson, M.O., Mudd, S.M., Pillans, B., Spooner, N.A., Fifield, L.K., Kirkby, M.J., Gloor, M., 2014. Quantifying the rate and depth dependence of bioturbation based on optically-stimulated luminescence (OSL) dates and meteoric ^{10}Be. Earth Surf. Process. Landf. 39, 1188–1196.

Kars, R., Wallinga, J., Cohen, K., 2008. A new approach towards anomalous fading correction for feldspar IRSL dating–tests on samples in field saturation. Radiat. Meas. 43, 786–790.

King, G.E., Guralnik, B., Valla, P.G., Herman, F., 2016a. Trapped-charge thermochronometry and thermometry: a status review. Chem. Geol. 446, 3–17.

King, G.E., Herman, F., Guralnik, B., 2016b. Northward migration of the eastern Himalayan syntaxis revealed by OSL thermochronometry. Science 353, 800–804.

King, G.E., Herman, F., Lambert, R., Valla, P.G., Guralnik, B., 2016c. Multi-OSL-thermochronometry of feldspar. Quat. Geochronol. 33, 76–87.

Kirk, J.T.O., 1994. The relationship between the inherent and the apparent optical properties of surface waters and its dependence on the shape of the volume scattering function. Ocean Optics. Oxford University Press, pp. 40–57 chapter.

Krbetschek, M.R., Götze, J., Dietrich, A., Trautmann, T., 1997. Spectral information from minerals relevant for luminescence dating. Radiat. Meas. 27, 695–748.

Lamothe, M., Auclair, M., Hamzaoui, C., Huot, S., 2003. Towards a prediction of long-term anomalous fading of feldspar IRSL. Radiat. Meas. 37, 493–498.
Lang, A., Moya, J., Corominas, J., Schrott, L., Dikau, R., 1999. Classic and new dating methods for assessing the temporal occurrence of mass movements. Geomorphology 30, 33–52.
Lehmann, B., Valla, P.G., King, G.E., Herman, F., 2018. Investigation of OSL surface exposure dating to reconstruct post-LIA glacier fluctuations in the French Alps (Mer de Glace, Mont Blanc massif). Quat. Geochronol. 44, 63–74.
Li, B., Li, S.H., 2011. Luminescence dating of K-feldspar from sediments: a protocol without anomalous fading correction. Quat. Geochronol. 6, 468–479.
Li, B., Li, S.H., 2013. The effect of band-tail states on the thermal stability of the infrared stimulated luminescence K-feldspar. J. Lumin. 136, 5–10.
Malatesta, L.C., Avouac, J.P., Brown, N.D., Breitenbach, S.F.M., Pan, J., Chevalier, M.L., Rhodes, E., D, S.-C., Zhang, W., Charreau, J., Lav'e, J., Blard, P.H., 2017. Lag and mixing during sediment transfer across the Tian Shan piedmont caused by climate-driven aggradation-incision cycles. Basin Res. 30, 613–635.
Martin, R.L., Barchyn, T.E., Hugenholtz, C.H., Jerolmack, D.J., 2013. Timescale dependence of aeolian sand flux observations under atmospheric turbulence. J. Geophys. Res. Atmos. 118, 9078–9092.
McGuire, C., Rhodes, E.J., 2015a. Determining fluvial sediment virtual velocity on the Mojave River using K-feldspar IRSL: initial assessment. Quat. Int. 362, 124–131.
McGuire, C., Rhodes, E.J., 2015b. Downstream MET-IRSL single-grain distributions in the Mojave River, southern California: Testing assumptions of a virtual velocity model. Quat. Geochronol. 30, 239–244.
Meyer, M.C., Gliganic, L.A., Jain, M., Sohbati, R., Schmidmair, D., 2018. Lithological controls on light penetration into rock surfaces–Implications for OSL and IRSL surface exposure dating. Radiat. Meas. 120, 298–304.
Morthekai, P., Thomas, J., Pandian, M.S., Balaram, V., Singhvi, A.K., 2012. Variable range hopping mechanism in band-tail states of feldspars: a time-resolved IRSL study. Radiat. Meas. 47, 857–863.
Mukul, M., Jaiswal, M., Singhvi, A.K., 2007. Timing of recent out-of-sequence active deformation in the frontal Himalayan wedge: Insights from the Darjiling sub-Himalaya, India. Geology 11, 999–1002.
Murray, A.S., Buylaert, J.P., Thomsen, K.J., Jain, M., 2009. The effect of preheating on the IRSL signal from feldspar. Radiat. Meas. 44, 554–559.
Olley, J.M., Murray, A., Roberts, R.G., 1996. The effects of disequilibria in the uranium and thorium decay chains on burial dose rates in fluvial sediments. Quat. Sci. Rev. 96, 751–760.
Ou, X.J., Roberts, H.M., Duller, G.A.T., Gunn, M.D., Perkins, W.T., 2018. Attenuation of light in different rock types and implications for rock surface luminescence dating. Radiat. Meas. 120, 305–311.
Pagonis, V., Brown, N.D., 2019. On the unchanging shape of thermoluminescence peaks in preheated feldspars: Implications for temperature sensing and thermochronometry. Radiat. Meas. 124, 19–28.
Peltzer, G., Brown, N.D., Mériaux, A.S., van der Woerd, J., Ryerson, F.J., Hollingsworth, J., 2020. Stable rate of slip along the Karakax Section of the Altyn Tagh Fault from observation of interglacial and postglacial offset morphology and surface dating. J. Geophys. Res. Solid Earth 125, e2019JB018893.
Porat, N., Levi, T., Weinberger, R., 2007. Possible resetting of quartz OSL signals during earthquakes: evidence from late Pleistocene injection dikes, Dead Sea basin, Israel. Quat. Geochronol. 2, 272–277.
Porat, N., Davidovich, U., Avni, Y., Avni, G., Gadot, Y., 2018. Using OSL measurements to decipher soil history in archaeological terraces, Judean Highlands, Israel. Land Degrad. Dev. 29, 643–650.
Preusser, F., Chithambo, M.L., Gotte, T., Martini, M., Ramseyer, K., Sendezera, E.J., Susino, G.J., Wintle, A.G., 2009. Quartz as a natural luminescence dosimeter. Earth Sci. Rev. 97, 184–214.
Preusser, F., Rufer, D., Schreurs, G., 2011. Direct dating of Quaternary phreatic maar eruptions by luminescence methods. Geology 39, 1135–1138.
Randall, J.T., Wilkins, M.H.F., 1945. Phosphorescence and electron traps I. The study of trap distributions. Proc. R. Soc. Lond. A 184, 366–389.
Reimann, T., Notenboom, P.D., Schipper, M.A.D., Wallinga, J., 2015. Testing for sufficient signal resetting during sediment transport using a polymineral multiple-signal luminescence approach. Quat. Geochronol. 25, 26–36.
Reimann, T., Roman-Sanchez, A., Vanwalleghem, T., Wallinga, J., 2017. Getting a grip on soil reworking–Single-grain feldspar luminescence as a novel tool to quantify soil reworking rates. Quat. Geochronol. 42, 1–14.
Reiners, P.W., Ehlers, T.A., Zeitler, P.K., 2005. Past, present, and future of thermochronology. Rev. Mineral. Geochem. 58, 1–18.
Rengers, F.K., Pagonis, V., Mahan, S.A., 2017. Can thermoluminescence be used to determine soil heating from a wildfire? Radiat. Meas. 107, 119–127.
Rhodes, E.J., 2011. Optically stimulated luminescence dating of sediments over the past 200,000 years. Annu. Rev. Earth Planet. Sci. 39, 461–488.
Rhodes, E.J., Farwig, V., Chappell, J., Pillans, B., 2004. Luminescence of single grain quartz grains to determine past movement and heating. Regolith. CRC LEME, pp. 295–298 chapter.
Rittenour, T.M., 2018. Dates and rates of Earth-surface processes revealed using luminescence dating. Elements 14, 21–26.
Rittenour, T.M., Riggs, N.R., Kennedy, L.E., 2012. Application of single-grain OSL to quartz xenocrysts within a basalt flow, San Francisco volcanic field, northern Arizona, USA. Quat. Geochronol. 10, 300–307.
Román-Sánchez, A., Laguna, A., Reimann, T., Giráldez, J.V., Peña, A., Vanwalleghem, T., 2019a. Bioturbation and erosion rates along the soil-hillslope conveyor belt, part 2: quantification using an analytical solution of the diffusion-advection equation. Earth Surf. Process. Landf. 44, 2066–2080.
Román-Sánchez, A., Reimann, T., Wallinga, J., Vanwalleghem, T., 2019b. Bioturbation and erosion rates along the soil-hillslope conveyor belt, part 1: insights from single-grain feldspar luminescence. Earth Surf. Process. Landf. 44, 2051–2065.
Rufer, D., Gnos, E., Mettier, R., Preusser, F., Schreurs, G., 2012. Proposing new approaches for dating young volcanic eruptions by luminescence methods. Geochronometria 39, 48–56.
Salisbury, J.B., Arrowsmith, J.R., Brown, N.D., Rockwell, R., Akciz, S., Ludwig, L.G., 2018. The age and origin of small offsets at Van Matre Ranch along the San Andreas Fault in the Carrizo Plain, California. Bull. Seismol. Soc. Am. 108, 639–653.
Sawakuchi, A.O., Guedes, C.C.F., DeWitt, R., Giannini, P.C.F., Blair, M.W., Nascimento, D.R., Faleiros, F.M., 2012. Quartz OSL sensitivity as a proxy for storm activity on the southern Brazilian coast during the Late Holocene. Quat. Geochronol. 13, 92–102.
Sawakuchi, A.O., Jain, M., Mineli, T.D., Nogueira, L., Bertassoli, D.J., Haggi, C., Sawakuchi, H. O., Pupim, F.N., Grohmann, C.H., Chiessi, C.M., Zabel, M., Mulitza, S., Mazoca, C.E.M., Cunha, D.F., 2018. Luminescence of quartz and feldspar fingerprints provenance and correlates with the source area denudation in the Amazon River basin. Earth Planet. Sci. Lett. 492, 152–162.
Schmidt, C., Friedrich, J., Zöller, L., 2015. Thermochronometry using red TL of quartz? Numerical simulation and observations from in-situ drill-hole samples. Radiat. Meas. 81, 98–103.
Schmidt, C., Schaarschmidt, M., Kolb, T., Büchel, G., Richter, D., Zöller, L., 2017a. Luminescence dating of Late Pleistocene eruptions in the Eifel Volcanic Field, Germany. J. Quat. Sci. 32, 628–638.
Schmidt, C., Tchouankoue, J.P., Nemzoue, P.N.N., Ayaba, F., Nformidah-Ndah, S.S., Chifu, E.N., 2017b. New thermoluminescence age estimates for the Nyos maar eruption (Cameroon Volcanic Line). PLoS One 12, 1–17.
Sellwood, E.L., Guralnik, B., Kook, M., Prasad, A.K., Sohbati, R., Hippe, K., Wallinga, J., Jain, M., 2019. Optical bleaching front in bedrock revealed by spatially-resolved infrared photoluminescence. Sci. Rep. 9, 2611.
Shen, Z., Tornqvist, T.E., Mauz, B., Chamberlain, E.L., Nijhuis, A.G., Sandoval, L., 2015. Episodic overbank deposition as a dominant mechanism of floodplain and delta-plain aggradation. Geology 43, 875–878.
Singhvi, A.K., Banerjee, D., Pande, K., Gogte, V., Valdiya, K.S., 1994. Luminescence studies on neotectonic events in South-Central Kumaun Himalaya: a feasibility study. Quat. Geochronol. 13, 595–600.
Smedley, R.K., Duller, G.A.T., Pearce, N.J.G., Roberts, H.M., 2012. Determining the K-content of single-grains of feldspar for luminescence dating. Radiat. Meas. 47, 790–796.
Sohbati, R., Murray, A.S., Jain, M., Buylaert, J.P., Thomsen, K.J., 2011. Investigating the resetting of OSL signals in rock surfaces. Geochronometria 38, 249–258.
Sohbati, R., Murray, A.S., Chapot, M.S., Jain, M., Pederson, J., 2012. Optically stimulated luminescence (OSL) as a chronometer for surface exposure dating. J. Geophys. Res. 117, B09202.
Sohbati, R., Murray, A.S., Porat, N., Jain, M., Avner, U., 2015. Age of a prehistoric "Rodedian" cult site constrained by sediment and rock surface luminescence dating techniques. Quat. Geochronol. 30, 90–99.
Sohbati, R., Liu, J., Jain, M., Murray, A., Egholm, D., Paris, R., Guralnik, B., 2018. Centennial- to millennial-scale hard rock erosion rates deduced from luminescence-depth profiles. Earth Planet. Sci. Lett. 493, 218–230.
Spencer, J.Q., Sanderson, D.C.W., 1994. Mapping thermal exposure by luminescence thermometry. Radiat. Meas. 23, 465–468.
Spencer, J.Q.G., Hadizadeh, J., Gratier, J.P., Doan, M.L., 2012. Dating deep? Luminescence studies of fault gouge from the San Andreas Fault zone 2.6 km beneath Earth's surface. Quat. Geochronol. 10, 280–284.
Spooner, N.A., Questiaux, D.G., 2000. Kinetics of red, blue and UV thermoluminescence and optically-stimulated luminescence from quartz. Radiat. Meas. 32, 659–666.
Stang, D.M., Rhodes, E.J., Heimsath, A.M., 2012. Assessing soil mixing processes and rates using a portable OSL-IRSL reader: preliminary determinations. Quat. Geochronol. 10, 314–319.
Stockmeyer, J.M., Shaw, J.H., Brown, N.D., Rhodes, E.J., Richardson, P.W., Wang, M., Lavin, L.C., Guan, S., 2017. Active thrust sheet deformation over multiple rupture cycles: a quantitative basis for relating terrace folds to fault slip rates. Geol. Soc. Am. Bull. 129, 1337–1356.
Stokes, S., Bray, H.E., Blum, M.D., 2001. Optical resetting in large drainage basins: tests of zeroing assumptions using single-aliquot procedures. Quat. Sci. Rev. 20, 879–885.
Summa-Nelson, M.C., Rittenour, T.M., 2012. Application of OSL dating to middle to late Holocene arroyo sediments in Kanab Creek, southern Utah, USA. Quat. Geochronol. 10, 167–174.
Thomsen, K.J., Murray, A.S., Jain, M., Bøtter-Jensen, L., 2008. Laboratory fading rates of various luminescence signals from feldspar-rich sediment extracts. Radiat. Meas. 43, 1474–1486.
Visocekas, R., Spooner, N.A., Zink, A., Blanc, P., 1994. Tunnel afterglow, fading and infrared emission in thermoluminescence of feldspars. Radiat. Meas. 23, 377–385.
Wintle, A., 1973. Anomalous fading of thermoluminescence in mineral samples. Nature 245, 143–144.
Zinke, R., Dolan, J.F., Rhodes, E.J., Dissen, R.V., McGuire, C.P., Hatem, A.E., Brown, N.D., Langridge, R.M., 2019. Multimillennial incremental slip rate variability of the Clarence Fault at the Tophouse Road Site, Marlborough Fault System, New Zealand. Geophys. Res. Lett. 46, 717–725.
Zular, A., Sawakuchi, A.O., Wang, H., Guedes, C.C.F., Hartman, G.A., Jaqueto, P.F., Chiessi, C. M., Cruz, F.W., Giannini, P.C.F., Daros, V.K., Atencio, D., Trindade, R.I.F., 2020. The response of a dune succession from Lençóis Maranhenses, NE Brazil, to climate changes between MIS 3 and MIS 2. Quat. Int. 537, 97–111.